Nanoscale

PAPER

View Article Online
View Journal | View Issue

Cite this: *Nanoscale*, 2015, **7**, 1037

Anisotropic conductive films based on highly aligned polyimide fibers containing hybrid materials of graphene nanoribbons and carbon nanotubes†

Mingkai Liu,[a,b] Yifeng Du,[a] Yue-E Miao,[a] Qianwei Ding,[a] Sixin He,[a] Weng Weei Tjiu,[c] Jisheng Pan[c] and Tianxi Liu*[a,b]

Anisotropic electrically conductive films (PI–GNR/CNT) consisting of highly aligned polyimide (PI) composite fibers with graphene nanoribbon (GNR) and carbon nanotube (CNT) (GNR/CNT) hybrids as nanofillers have been prepared by electrospinning. The GNR/CNT hybrids used here were prepared by one-step partial unzipping of multi-walled CNTs, in which, with the residual CNTs bonded on the randomly arranged GNR sheets, not only the aggregation of GNR sheets was greatly prevented but also an electrically conductive pathway with good conductivity was effectively formed with the CNTs acting as linking bridges between different GNRs. Due to the three-dimensional (3D) conductive network structure of the GNR/CNT hybrid and fine dispersion and alignment inside the PI fibers, as well as the good interfacial interaction between the GNR/CNT hybrid and the PI matrix, PI–GNR/CNT composite films exhibit a unique property of anisotropic electrical conductivity of 8.3×10^{-2} S cm^{-1} in the parallel direction along the fibers and 7.2×10^{-8} S cm^{-1} in the perpendicular direction, which may open the way for wide potential applications of anisotropic conductive nanomaterials in practical production and scientific research fields.

Received 16th October 2014,
Accepted 19th November 2014

DOI: 10.1039/c4nr06117a

www.rsc.org/nanoscale

1. Introduction

Anisotropic materials, with distinct properties in each direction, have attracted tremendous attention in recent years for their important applications such as magnetic devices, electronic sensors and field-emission devices.[1–3] A typical and representative example of the anisotropic materials is magnetic materials, which have already been widely used in the fields of electricity, optics, and so on.[4,5] Recently, polymer-based anisotropic electrically conductive materials with hierarchical architecture and excellent anisotropic properties have been fabricated. Giannelis and coworkers have prepared graphene–Nafion nanocomposites by a two-step approach of casting and reduction, achieving the successful preparation of well-aligned graphene nanosheets with excellent anisotropic electrical conductivity.[6] Zhu and coworkers have prepared tailored parallel graphene stripes in a plastic film by shear-induced self-assembly with almost four orders of magnitude difference of conductivity in parallel and perpendicular directions.[7] However, the complicated manufacturing process and sophisticated fabricating facilities for preparing anisotropic materials make it difficult for mass production. Therefore, developing a simple, low-cost and mass production method for preparing anisotropic electrically conductive materials is urgent and of great importance.

Currently, the most investigated anisotropic electrically conductive composites are usually prepared based on the polymer matrices such as polyethylene,[3] polypropylene,[7] poly(dimethylsiloxane),[2] and copolymers of polystyrene-poly(4-vinyl pyridine),[8] due to their high strength, light weight, corrosion resistance and insulation properties. Among the most commonly used polymers, polyimide (PI), which is considered as a kind of high-performance engineering polymer, has attracted tremendous interest from researchers and has been investigated in many practical application fields due to its superior properties, such as outstanding

[a]*State Key Laboratory of Molecular Engineering of Polymers, Department of Macromolecular Science, Fudan University, Shanghai 200433, P. R. China. E-mail: txliu@fudan.edu.cn; Fax: +86-21-65640293; Tel: +86-21-55664197*
[b]*School of Chemistry and Chemical Engineering and Jiangsu Key Laboratory of Green Synthetic Chemistry for Functional Materials, Jiangsu Normal University, Xuzhou 221116, P. R. China*
[c]*Institute of Materials Research and Engineering, A*STAR (Agency for Science, Technology and Research), 3 Research Link, Singapore, 117602, Singapore*
†Electronic supplementary information (ESI) available. See DOI: 10.1039/c4nr06117a

mechanical properties, excellent thermal stability, as well as low dielectric constant.[9–12] PI-based composite materials with excellent performance are urgently needed in many practical application fields. Recently, much effort has been made to improve the performance of PI-based composites by chemical/physical interfacial modification. For example, properties such as mechanical strength and toughness, electrical conductivity and thermal stability of PI have been significantly improved by addition of a small amount of graphene due to the good dispersion of graphene and the excellent interfacial interaction between graphene sheets and the PI matrix.[13–16]

Carbon nanotubes (CNTs) with small size, high surface area, large aspect ratio and high electrical/thermal conductivity have been considered as an attractive option for applications in sensors,[17] field-effect transistors,[18,19] energy storage devices,[20–23] and conductive composite materials,[3,24] also another superb carbon material, graphene, with a single atom thick layer and hexagonal structural arrangement in a two-dimensional lattice, has attracted great attention in various practical application areas for its extraordinary properties such as large surface area, excellent mechanical flexibility, fast electron transportation, as well as superior thermal/chemical stability.[25–27] Interestingly, hybrid materials of graphene and CNTs with appreciatively interfacial interactions have recently been confirmed to be a very promising type of carbon material with superior electrical and optical performance to individual components, CNTs or graphene.[28,29] The effective hybridization of graphene and CNTs not only can promote the building-up of a three-dimensional (3D) conductive network, but also can decrease the tendency of aggregation of both graphene and CNTs. Furthermore, CNTs in the graphene/CNT hybrid can play an important role in accelerating the electron-transporting efficiency by acting as conductive bridges between graphene sheets.[30,31] Therefore, when used as nanofillers, the graphene/CNT hybrids can also increase the electrical and thermal conductivity of the polymer-based composites,[32,33] and furthermore markedly increase the dielectric property, toughness as well as thermal stability of the polymer matrices.[34–36]

In this work, anisotropic electrically conductive films consisting of highly aligned PI–GNR/CNT composite fibers have been fabricated by electrospinning with 3D hierarchical hybrids of graphene nanoribbons (GNRs) and CNTs (GNR/CNT) as conductive nanofillers. Here, GNR/CNT hybrids have been facilely prepared by partial unzipping of multi-walled CNTs. When exfoliated from mother-CNTs, the as-prepared GNR sheets have intact interactions with residual CNTs. Moreover, with CNTs acting as connecting bridges between different GNR sheets, an electrically conductive pathway was effectively built inside GNR/CNT hybrids. Therefore, the PI–GNR/CNT film shows a unique anisotropic electrical conductivity as well as good mechanical stability, as a result of the good dispersion of the GNR/CNT hybrid inside PI fibers and the superior mechanical properties of the PI matrix.

2. Experimental section

2.1 Materials

Pristine CNTs (diameter of 20–30 nm, 30 μm in length) were purchased from Chengdu Organic Chemicals Co. Ltd. Benzophenone-3,3,4,4-tetracarboxylic dianhydride (BTDA), 4,4′-diaminodiphenyl ether (DPE), *N*,*N*′-dimethylacetamide (DMAc), sulfuric acid (H_2SO_4, 98 wt%), phosphoric acid (H_3PO_4, 30 wt%), potassium permanganate ($KMnO_4$), hydrochloric acid (HCl, 36 wt%), and hydroiodic acid ($HI{\cdot}H_2O$, 45 wt%) were purchased from China Medicine Co. Ltd. All the reactants were used directly in the experiments without any further purification. Ultraclean water was used throughout the experiments.

2.2 Preparation of the GNR/CNT hybrid

The GNR/CNT hybrid was synthesized by partial longitudinal unzipping of pristine multi-walled CNTs (MWCNTs) according to our previous reports.[37,38] Typically, 150 mg of MWCNTs were dispersed in 40 mL H_2SO_4 and moderately stirred for 1 h. H_3PO_4 (4 mL) was gradually added into the reacting system and stirred for 15 min at room temperature. 450 mg of $KMnO_4$ was added into the mixture in batches of 150 mg every hour. Then, the temperature of the reaction system was increased to 70 °C and kept constant for 2 h followed by natural cooling to room temperature. The cooled mixture was poured into 100 mL of ice-water containing 4 mL of H_2O_2 (30 wt%) and allowed to coagulate for 12 h. Then, the obtained precipitate was washed with HCl (20 wt%) 2 times (10 mL each time) and dialyzed against ultraclean water for 1 week, resulting in the formation of an oxide GNR/CNT hybrid. The oxide GNR/CNT hybrid was reduced with $HI{\cdot}H_2O$ (98 °C for 10 h) to remove the redundant oxygen-containing groups in order to prepare GNR/CNT hybrid materials. After being washed 5 times, a stable dispersion of the GNR/CNT hybrid in DMAc was achieved.

2.3 Fabrication of PI–GNR/CNT composite films

Firstly, poly(amide acid) (PAA), the precursor of PI, was synthesized from BTDA and DPE with an equivalent molar ratio (as shown in Fig. 1). The mixture of BTDA and DPE was stirred at 320 rpm in DMAc solution at 0 °C, resulting in the formation of the PAA material by means of polycondensation reaction with the solid content of PAA in DMAc solution being about 15 wt%.

For preparation of PAA-GNR/CNT composite materials, the obtained GNR/CNT hybrids were imbedded into the PAA solution by rapid stirring, in which the content of GNR/CNT in the PAA-GNR/CNT composite can be simply but effectively adjusted by changing the amount of imbedded GNR/CNT hybrids (0.5 wt% to 9 wt% in this work). The as-prepared PAA-GNR/CNT composite solutions were used to prepare PAA-GNR/CNT fibers by the electrospinning technique at an applied voltage of 15 kV and a feeding rate of 1 mL h^{-1}. A specific rotating collector with a linear speed of 25 m s^{-1} was set up in order to effectively align the ejected PAA-GNR/CNT fibers. The obtained PAA-GNR/CNT fiber films were dried

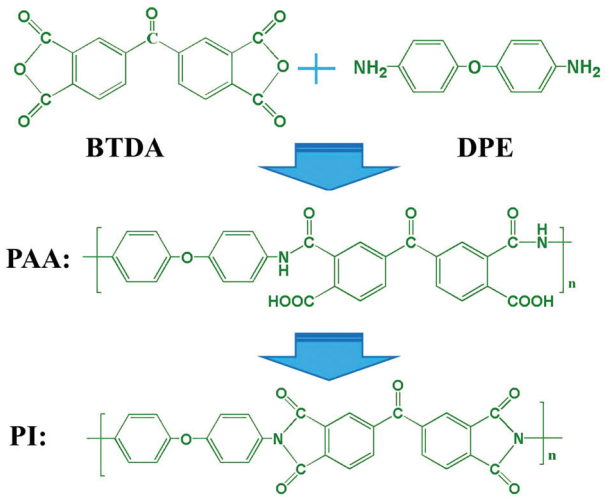

Fig. 1 Reaction scheme for preparation of PAA and PI by BTDA and DPE.

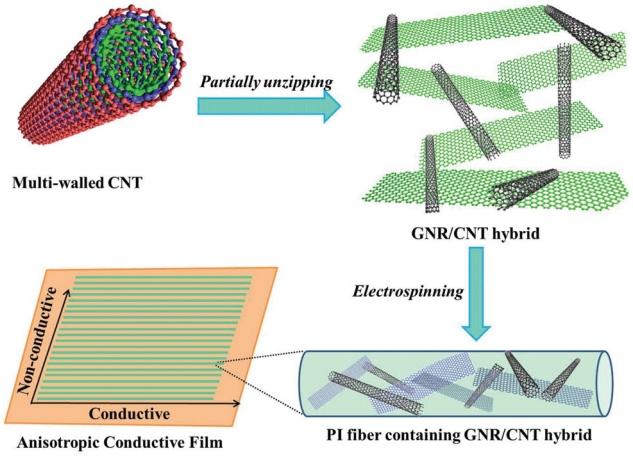

Fig. 2 Schematic showing the fabrication of free-standing anisotropic electrically conductive PI–GNR/CNT films with GNR/CNT hybrid as a nanofiller.

at 70 °C for 3 h in order to remove the residual solvent before being heated to 100 °C, 200 °C and 300 °C (maintained for 30 min at each stage) at a speed of 5 °C min^{-1} to complete the imidization process, achieving PI–GNR/CNT fiber films.

2.4 Characterization

Transmission electron microscopy (TEM, Jeol JEM2100) with an accelerating voltage of 200 kV was used to observe the morphology of pristine MWCNTs, GNR/CNT hybrids, as well as PI and PI–GNR/CNT fibers. Scanning electron microscopy (SEM, Zeiss, ultra 55) observations were performed on a Zeiss Ultra 55 instrument with an accelerating voltage of 5 kV in order to study the microstructures of the obtained fibers. X-ray diffraction (XRD) measurements were conducted using a PANalytical (X'Pert PRO) X-ray diffractometer with Cu Kα radiation (λ = 0.1542 nm; cathode current, 40 mA; operating energy, 40 keV). X-ray photoelectron spectroscopy (XPS) observations were conducted on a VG ESCALAB 220I-XL device. Fourier transform infrared (FTIR) analysis was performed on a Nicolet Nexus 470 FTIR spectrometer with a DTGS detector by signal-averaging 64 scans at a resolution of 4 cm^{-1}. The electrical conductivity of the samples was measured using a Keithley 4200 semiconductor system at room temperature. In the head portion of the tested films, the outer layer PI matrix was removed with O_2 plasma, and silver paste was used to coat the exposed surface of PI–GNR/CNT films to reduce the contact resistance between the metal leads and the tested samples. Characterization was performed in a linear sweep from −10 to 10 V, and the size of the tested film was about 5 mm × 5 mm.

3. Results and discussion

Fig. 2 shows the fabricating process of a PI–GNR/CNT anisotropic electrically conductive film with GNR/CNT hybrids as the nanofiller. Pristine MWCNTs with a length of 30 μm were partially unzipped, and the obtained GNR sheets by partial unzipping were exfoliated from the pristine mother-CNTs with the assistance of ultrasonication. The GNR sheets were co-dispersed with the residual CNTs in the organic solvent DMAc, resulting in the formation of 3D hybrid materials of CNTs (1D) and GNR (2D) sheets with a hierarchical structure. Here, the residual CNTs with a large aspect ratio were bonded on different GNR sheets and acted as "connecting bridges", forming crosslinked or inter-clocked architectures of CNT/GNR hybrids, which will effectively facilitate the electron or charge transfer inside this new carbon material. With the assistance of electrospinning, free-standing films consisting of highly aligned PI–GNR/CNT fibers can be prepared on a rotating roll collector. High content and uniformly dispersed GNR/CNT hybrid inside PI fibers endows PI–GNR/CNT composite films with great electrical conductivity along the aligned PI–GNR/CNT fibers. Furthermore, the outer layer of the PI matrix plays an important role in packaging the inner conductive materials, resulting in the effective impediment of the lateral transfer of electrons. This feature will efficiently promote the unidirectional transmission of electrons inside the PI–GNR/CNT fibers, resulting in the formation of PI-based fiber films with a unique property of anisotropic electrical conductivity.

Fig. 3 shows the TEM images of pristine CNTs and the prepared GNR/CNT hybrids. It is noted that pristine CNTs (Fig. 3a) have a large aspect ratio and relatively smooth edges with 15–20 side walls, as shown in Fig. 3b. Compared with the pristine CNTs, GNR sheets with an enlarged width can be vividly observed beside the residual CNTs, as shown in Fig. 3c. The prepared GNR sheets were homogeneously co-dispersed with the residual CNTs without apparent aggregation, with the residual CNTs linked with GNR sheets or bonded on different GNR sheets. Detailed information can be obtained from the image with high magnification (Fig. 3d). By acting as the

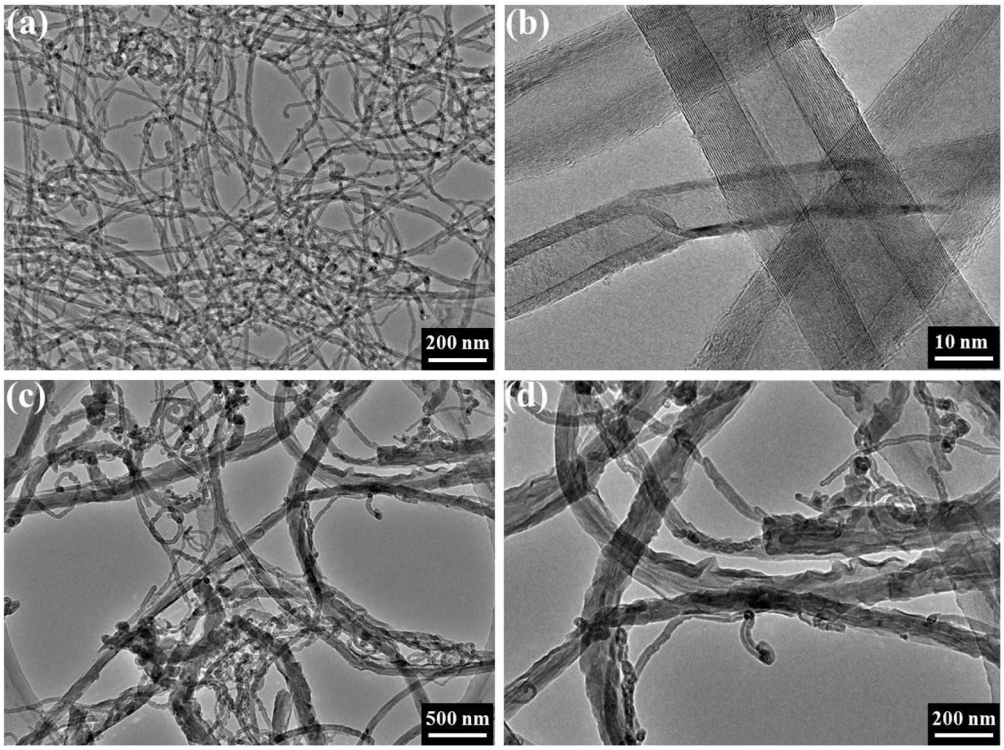

Fig. 3 TEM images of (a) pristine MWCNTs and (c) GNR/CNT hybrid. (b) and (d) are detailed TEM images of (a) and (c) under high magnifications, respectively.

connecting bridges, the residual CNTs not only prevent the aggregation of GNR sheets but also greatly enhance the electrical conductivity of the hybrid material by facilitating the charge transfer ability. This internally generated GNR/CNT hybrids endow themselves with a superior cross-linked hierarchical structure and an interfacial interaction between GNRs and CNTs compared to the physically mixed blend of graphene and CNTs, resulting in rapid electron transfer inside the GNR/CNT hybrid and a better interfacial catalyst than graphene or CNTs or their mixture.[37] This structural evolution can be further confirmed by SEM observations, as shown in Fig. S1.† The pristine CNTs show uniform tube-like structures without the other component existing. Compared with pristine CNTs, the GNR/CNT hybrid apparently consisted of two kinds of materials: GNR sheets and tube-like CNTs. As a matter of fact, these results adequately confirm that pristine CNTs were partially unzipped and the obtained GNR sheets were co-dispersed with the residual CNTs, resulting in the formation of 3D hybrid materials with hierarchical structures.

As oxygen containing groups will be inevitably introduced onto the surface or edges of unzipped GNR sheets and the residual CNTs, oxide GNR/CNT hybrids were first obtained after being treated by an unzipping process. X-ray diffraction (XRD) measurements of pristine CNTs, oxide GNR/CNT and GNR/CNT hybrids were carried out to detect the structural evolution of the prepared samples, as shown in Fig. 4. The pattern of pristine CNTs shows a sharp diffraction peak at about $2\theta = 26.1°$, corresponding to the good crystalline form of

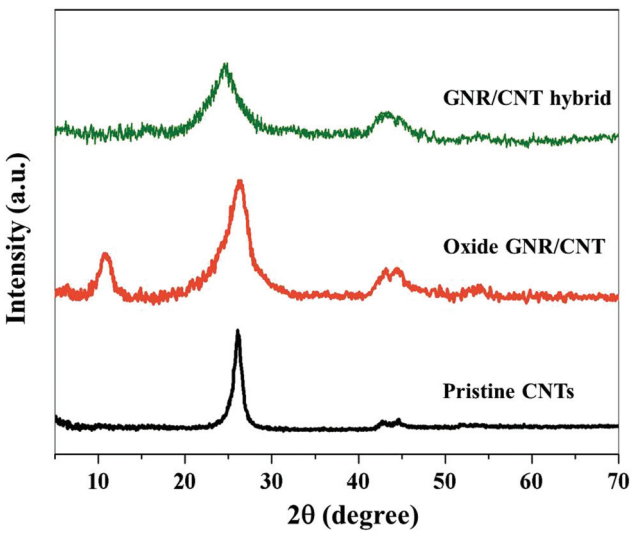

Fig. 4 XRD patterns of pristine CNTs, oxide GNR/CNT, and GNR/GNR hybrid.

CNTs with an interlayer spacing of 3.4 Å. After being partially unzipped, a new diffraction peak centered at about $2\theta = 10.9°$ was observed, confirming the successful exfoliation of GNR sheets from pristine CNTs, which is comparable to the result of graphene oxide reported in the literature.[39,40] Furthermore, the obtained oxide GNR/CNT hybrid was reduced with $HI{\cdot}H_2O$ at 98 °C for 10 h. It can be seen that the characteristic diffrac-

tion peak of oxide GNR sheets disappeared as a result of the effective removal of oxygen containing groups. The successful chemical reduction of oxide GNR/CNT can be further confirmed by FTIR analysis, as shown in Fig. S2.† All samples exhibit a broad characteristic absorption peak at about 3440 cm^{-1}, which can be attributed to the adsorbed bound water or the hydroxyl group on the basic sites of the samples.[41] Compared with pristine CNTs, apparent vibration peaks at 1720 cm^{-1} (C═O carboxyl stretching vibration), 1227 cm^{-1} (C–OH stretching vibration) and 1060 cm^{-1} (C–O–C stretching vibration) were observed in the spectra of the oxide GNR/CNT hybrid sample. From another perspective, these introduced oxygen-containing groups can factually demonstrate the unzipping of side walls of pristine CNTs. After reduction, the FTIR spectra of the GNR/CNT hybrid show very weak or diminished vibration peaks of oxygen-containing groups, which can be ascribed to the effective reduction with $HI{\cdot}H_2O$. Furthermore, the dispersibility of several samples was tested, as shown in Fig. S3.† The pristine CNTs were quickly aggregated in water due to their large number of conjugated structures. The obtained oxide GNR/CNT hybrid has a favorable dispersion ability in water, which can be ascribed to the assistance of the introduced oxygen-containing groups on the surface of GNRs and CNTs. After being chemically reduced, the GNR/CNT hybrid also precipitated, which confirms the efficient removal of oxygen-containing groups. Interestingly, the obtained GNR/CNT hybrid has perfect dispersion stability in the solvent DMAc, which ensures good mixing and sufficient dispersion of the GNR/CNT hybrid throughout the prepared PAA matrix in the same solvent.

PI based composite films with unique properties and hierarchical microscopic structures have been prepared and reported recently, such as PI/graphene nanocomposite films prepared by *in situ* polymerization,[42] PI/graphene films with graphene sheets highly aligned along the film surface,[15] as well as surface-conductive PI films prepared *via in situ* codeposition of conductive metal salts.[43] However, fully anisotropic electrically conductive PI based films with total wrapping of conductive nanofillers with the PI matrix have not been prepared. We believe that highly aligned PI nanofibers prepared by electrospinning with conductive nanofillers can open the way for fabricating anisotropic electrically conductive PI films. In this work, the GNR/CNT hybrid was used as a nanofiller inside PI fibers to fabricate aligned PI–GNR/CNT composite fibers (Fig. 5). Fig. 5a shows randomly arranged PI–GNR/CNT fibers obtained *via* electrospinning. With the assistance of a rotation disc device, highly aligned pure PI fibers with uniform diameter and smooth surface were collected, as

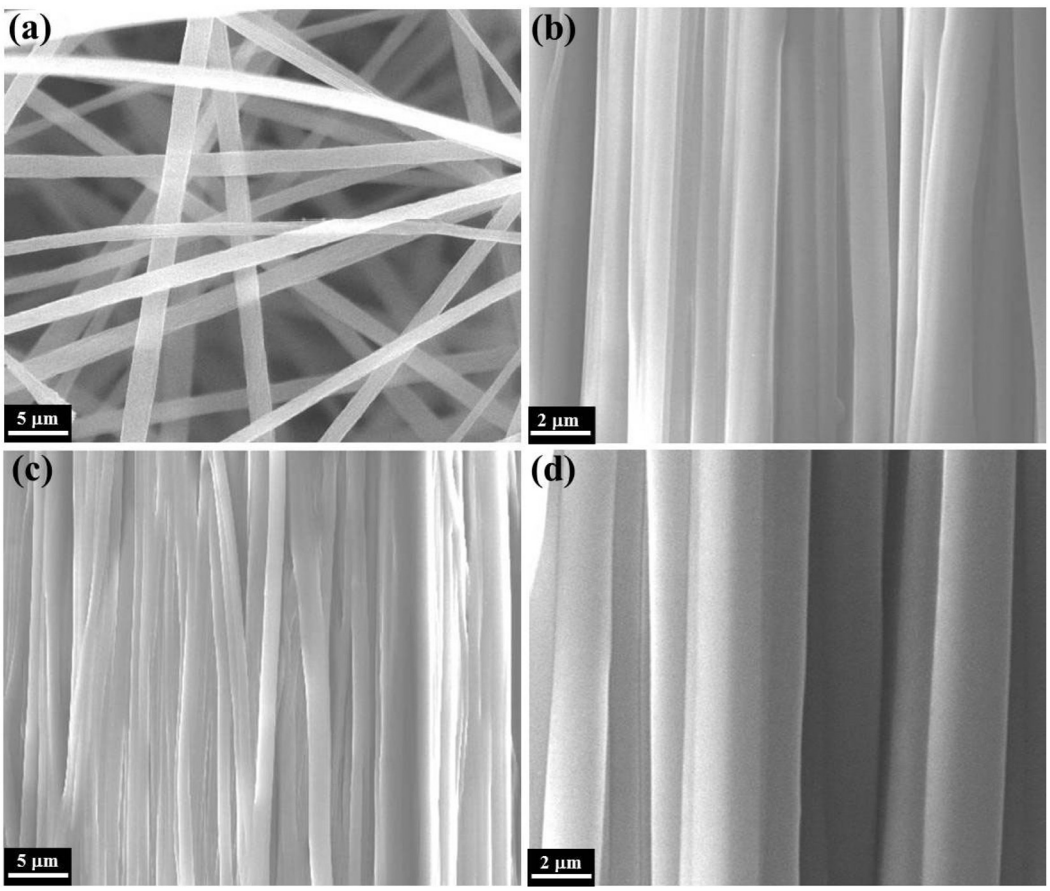

Fig. 5 SEM images of randomly arranged PI–GNR/CNT fibers (a), pure PI fibers with high alignment (b), and highly aligned PI–GNR/CNT composite fibers at low (c) and high (d) magnifications.

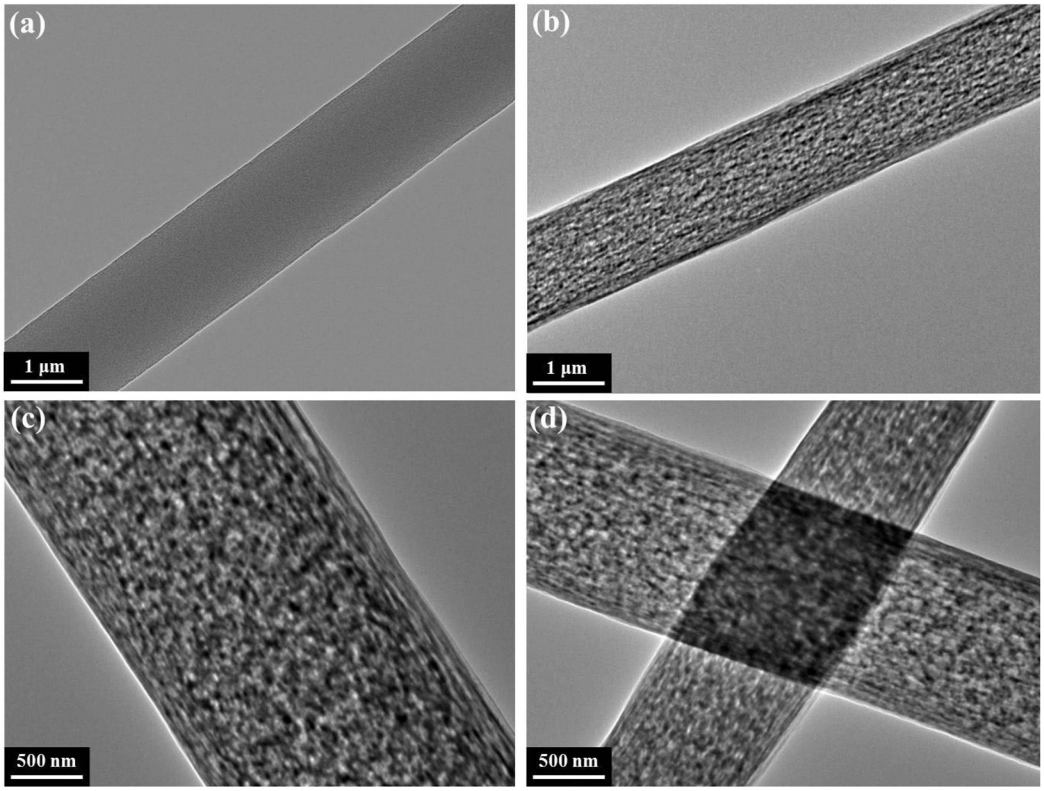

Fig. 6 TEM images of pure PI fiber (a), PI–GNR/CNT fibers at low (b) and high (c) magnifications, as well as the cross section of PI–GNR/CNT fibers (d).

shown in Fig. 5b. The collected PI fiber shows an average diameter of 2 μm, which is much larger than previously reported polymer fibers by electrospinning.[44–46] This enlarged diameter is favorable for preparing conductive PI–GNR/CNT composite fibers by providing a vast space for the assembly of the 3D GNR/CNT hybrid. With quick rotation, a film of PI–GNR/CNT fibers with high alignment was collected, as shown in Fig. 5c and d. No bead was formed on the surface of the fibers with the diameter of PI–GNR/CNT fibers uniformly distributed, which is very important for the preparation of high-performance PI–GNR/CNT composites by avoiding the emergence of defects and stress concentration points.

TEM observations were used to further demonstrate the successful hybridization of the GNR/CNT hybrid with PI fibers. For comparison, a pure PI fiber showing smooth edges with no fillers can be observed throughout its intrinsic space (as shown in Fig. 6a), which proves that the PI matrix used in this work has good fiber formability. PI–GNR/CNT composite fibers have also been successfully prepared with the assistance of the electrospinning technique (Fig. 6b and c). It can be clearly seen that GNR/CNT hybrid materials were uniformly dispersed throughout PI fibers with no beads observed. The excellent dispersion of GNR/CNT hybrids even at high loading contents can greatly promote the construction of an electrically conductive pathway inside PI fibers, which further contributes to the fabrication of anisotropic electrically conductive films based on PI–GNR/CNT composites. Moreover, the external PI matrix can play an important role in tightly wrapping the internal GNR/CNT hybrid materials, with no integration of the conductive GNR/CNT hybrids even when two PI–GNR/CNT fibers were cross-stacked (as shown in Fig. 6d), which are favorable features for the preparation of anisotropic conductive PI–GNR/CNT films.

The electrical conductivity of PI–GNR/CNT composite films was measured using a Keithley semiconductor measurement system at ambient temperature. It can be seen in Fig. 7 that there is a current signal in the parallel direction along the aligned PI–GNR/CNT fibers, which proves that the successful introduction of the 3D conductive material of GNR/CNT into PI fibers provides good electrical conductivity to these PI–GNR/CNT fibers. The corresponding current density along the parallel direction of aligned PI–GNR/CNT fibers was gradually increased with the content of GNR/CNT hybrids increasing, confirming that the electrical conductivity of PI–GNR/CNT composite films was constructively impacted by the content of GNR/CNT nanofillers. When the content of the GNR/CNT hybrid in PI–GNR/CNT composites was increased to 9%, a high electrical conductivity of 8.3×10^{-3} S cm^{-1} was achieved, which is much higher than the inherent electrical conductivity of the PI material (10^{-14} S cm^{-1}).[15] The greatly enhanced electrical conductivity of the PI–GNR/CNT composite film can be ascribed to the synergistic and multiple actions of high content and perfect dispersion of GNR/CNT nanofillers inside PI fibers, and the excellent electrical conductivity of the 3D

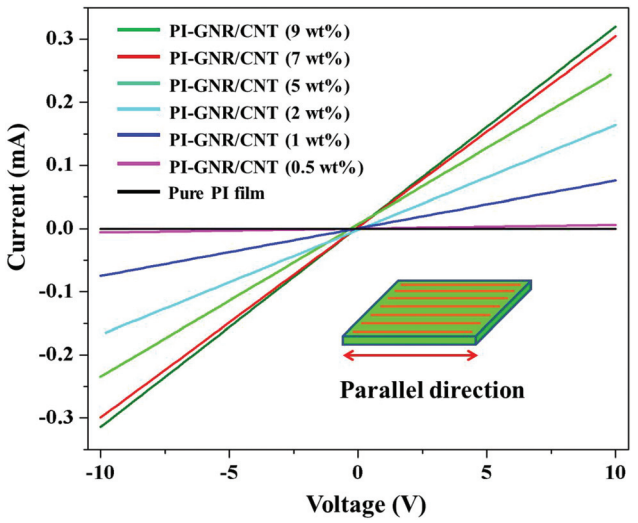

Fig. 7 *I–V* curves of pure PI film and PI–GNR/CNT composite films with different mass fraction of GNR/CNT fillers from 0.5 to 9 wt%.

conductive network constructed from crosslinked GNRs and CNTs. Here, the good dispersion of the GNR/CNT hybrid inside PI fibers can be ascribed to the interfacial interaction between the GNR/CNT hybrid and the hydroxyl groups on the diamine monomer. The good electrical conductivity of the PI–GNR/CNT fiber film can also be ascribed to the efficient reduction with HI·H_2O of the oxide GNR/CNT hybrid, as confirmed by XPS observations in Fig. 8. The oxide GNR/CNT sample shows apparent oxygen-containing groups, including C═O (288.3 eV) and C–O (286.5 eV) groups, which were introduced in the unzipping process.[47,48] After reducing with HI·H_2O, it can be obviously observed that the C–O/C═O peaks were significantly decreased, which means the oxygen-containing groups were greatly removed and the aromatic structure of GNRs and CNTs has been recovered.

To confirm the anisotropic conductive property of the obtained PI–GNR/CNT film, the electrical conductivity of the PI–GNR/CNT film at two cross-directions (parallel and perpendicular directions, as shown in Fig. 9a) was measured. Fig. 9b shows the *I–V* curves of the PI–GNR/CNT (9 wt%) sample obtained from the Keithley system, with the red and blue lines representing the current–voltage response at different directions as shown in Fig. 9a. It can be seen that the corresponding current intensity in the parallel direction is about 6 orders of magnitude higher than that in the perpendicular direction, which means that this PI–GNR/CNT (9 wt%) film has significantly different current signals in orthogonal directions. The calculated electrical conductivity in the parallel direction of the PI–GNR/CNT film is about 8.3 × 10^{-2} S m^{-1},

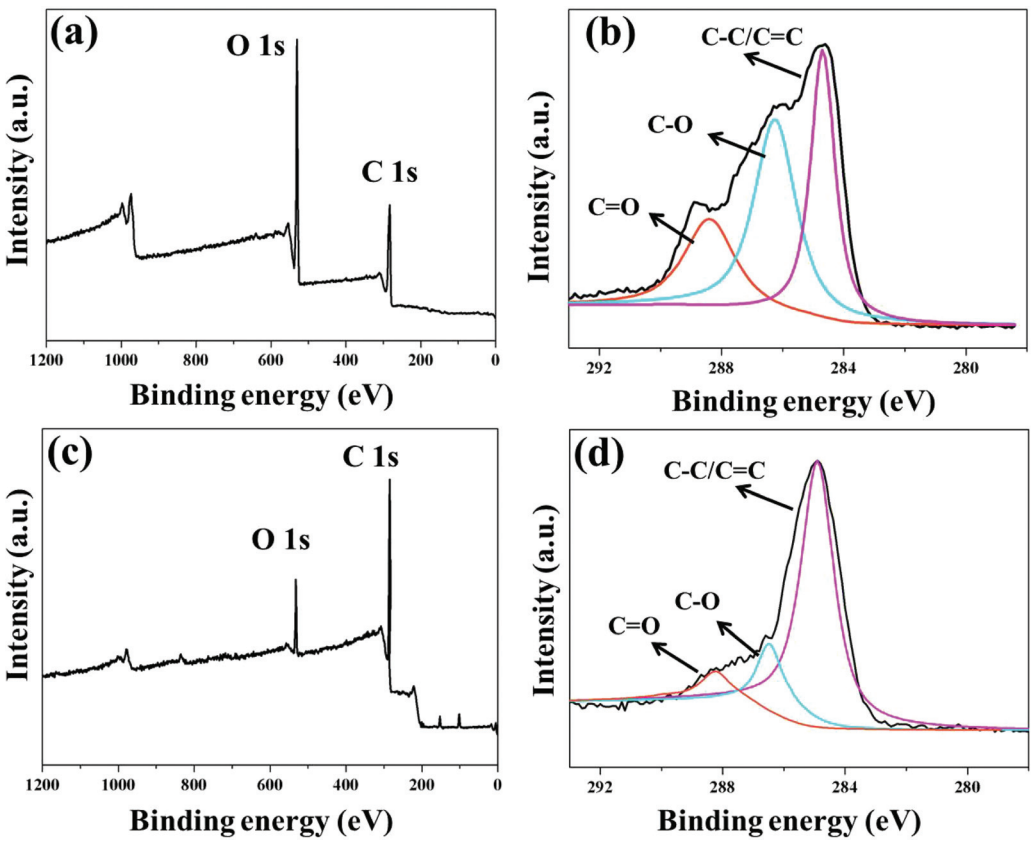

Fig. 8 XPS survey spectra of the oxide GNR/CNT hybrid (a and b), and pure GNR/CNT hybrid (c and d), (b) and (d) are the corresponding C 1s spectra of (a) and (c).

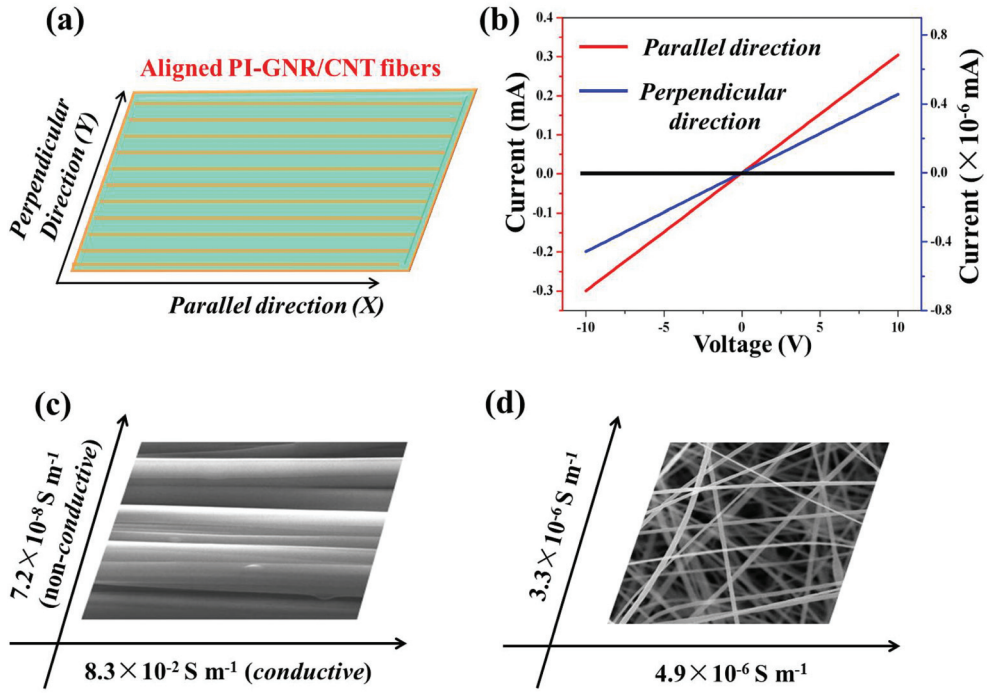

Fig. 9 (a) Illustration shows the parallel and perpendicular directions of aligned PI–GNR/CNT fibers in the composite film; (b) corresponding *I–V* curves of the PI–GNR/CNT (9 wt%) film measured at parallel and perpendicular directions; calculated electrical conductivity from the obtained *I–V* curves of highly aligned (c) and randomly oriented (d) PI–GNR/CNT composite fiber films.

which is higher than the antistatic criterion value of 10^{-6} S m^{-1}.[49] This result proves that the complete embedding of the GNR/CNT hybrid in PI fibers provides good electrically conductive property to PI–GNR/CNT fibers by forming a conductive pathway with interfacial contact between GNRs and CNTs. However, insulating behavior is observed from the *I–V* curve in the perpendicular direction as the electrical conductivity is about 7.2×10^{-8} S m^{-1}. Compared with the high conductivity value of 8.3×10^{-2} S m^{-1} in the parallel direction, it is known that the PI-based film with a unique property of anisotropic electrically conductivity was obtained. Here, the insulating behavior in the perpendicular direction can be attributed to the tight wrapping effect of the outer PI matrix, as shown in Fig. S4† (indicated by the arrows). Similar electrically conductivity tests were also performed on the randomly oriented PI–GNR/CNT composite fiber films. As shown in Fig. 9d, no apparent difference of electrical conductivity in different directions can be observed (3.3×10^{-6} S m^{-1} and 4.9×10^{-6} S m^{-1} in two crossed directions, respectively). This result can strongly confirm the significant contribution of the high orientation of PI–GNR/CNT fibers to the unique property of anisotropic electrically conductivity of PI-based composite films. Due to the excellent mechanical properties of the PI matrix,[50–53] perfect electrical conductivity of the 3D GNR/CNT hybrid, as well as good interfacial interaction between the GNR/CNT and the PI matrix, the conductivity of the PI–GNR/CNT film was scarcely decreased even after 100 repetitions of bending at 90 degrees, as shown in Fig. 10. A digital photograph of the flexible PI–GNR/CNT (9 wt%) composite film upon bending is provided (Fig. S5†). All these findings indicate that the prepared PI–GNR/CNT composite film not only has a good property of anisotropic conductivity, but also exhibits excellent resistance to mechanical deformation.

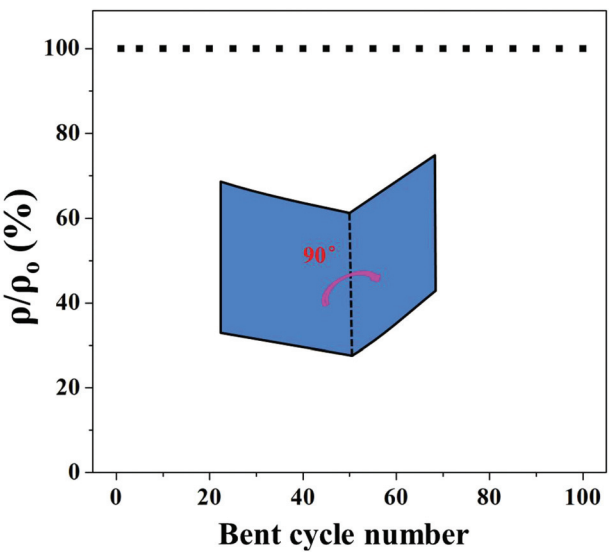

Fig. 10 The electrical conductivity dependence on the bent cycle number for a flexible PI–GNR/CNT (9 wt%) composite film during the bending process, ρ_o and ρ represent the conductivity of the film before and after bending, respectively.

4. Conclusion

In summary, we succeeded in fabrication of a PI–GNR/CNT composite film with unique properties of anisotropic conductivity and good stability by embedding 3D conductive hybrid materials of GNR/CNT into highly aligned PI fibers. Particularly, the GNR/CNT hybrid used here was simply but efficiently prepared by one-step partial unzipping of pristine MWCNTs, achieving the cross-linked conductive network of CNTs bridged by GNRs, also an interconnected conductive structure of 3D GNR/CNT can be developed inside PI fibers due to the high content and perfect dispersion stability of the GNR/CNT hybrid. This flexible PI–GNR/CNT film exhibits good anisotropic conductive performance with a difference of 6 orders of magnitude in parallel (8.3×10^{-2} S m^{-1}) and perpendicular (7.2×10^{-8} S m^{-1}) directions of the aligned PI–GNR/CNT fibers. Furthermore, this PI–GNR/CNT composite film can be mass produced due to the facile electrospinning technology and efficient method for preparing GNR/CNT hybrids. Moreover, this effective hybridization of the GNR/CNT hybrid into highly aligned PI fibers opens up good opportunities for preparing anisotropic conductive materials based on organic–inorganic systems.

Acknowledgements

The authors are grateful for the financial support from the National Natural Science Foundation of China (51125011, 51373037, 51433001).

References

1 G. H. Yu, A. Y. Cao and C. M. Lieber, *Nat. Nanotechnol.*, 2007, **2**, 372–377.
2 Y. J. Jung, S. Kar, S. Talapatra, C. Soldano, G. Viswanathan, X. S. Li, Z. L. Yao, F. S. Ou, A. Avadhanula, R. Vajtai, S. Curran, O. Nalamasu and P. M. Ajayan, *Nano Lett.*, 2006, **6**, 413–418.
3 J. F. Gao, D. X. Yan, B. Yuan, H. D. Huang and Z. M. Li, *Compos. Sci. Technol.*, 2010, **70**, 1973–1979.
4 J. H. Shen, Y. H. Zhu, K. F. Zhou, X. L. Yang and C. Z. Li, *J. Mater. Chem.*, 2012, **22**, 545–550.
5 A. J. Amali, P. Saravanan and R. K. Rana, *Angew. Chem., Int. Ed.*, 2011, **50**, 1318–1321.
6 S. Ansari, A. Kelarakis, L. Estevez and E. P. Giannelis, *Small*, 2010, **6**, 205–209.
7 C. Mao, J. R. Huang, Y. T. Zhu, W. Jiang, Q. X. Tang and X. J. Ma, *J. Phys. Chem. Lett.*, 2013, **4**, 43–47.
8 S. H. Yun, S. M. Yoo, B. H. Sohn, J. C. Jung, W. C. Zin, S. Y. Kwak and T. S. Lee, *Langmuir*, 2005, **21**, 3625–3628.
9 D. Chen, Y. E. Miao and T. X. Liu, *ACS Appl. Mater. Interfaces*, 2013, **5**, 1206–1212.
10 X. W. Peng, Q. Wu, S. H. Jiang, M. Hanif, S. L. Chen and H. Q. Hou, *Mater. Lett.*, 2014, **133**, 240–242.
11 S. L. Chen, P. Hu, A. Greiner, C. Y. Cheng, H. F. Cheng, F. F. Chen and H. Q. Hou, *Nanotechnology*, 2008, **19**, 015604.
12 W. H. Xu, Y. C. Ding, S. H. Jiang, L. L. Chen, X. J. Liao and H. Q. Hou, *Mater. Lett.*, 2014, **135**, 158–161.
13 M. Yoonessi, Y. Shi, D. A. Scheiman, M. Lebron-Colon, D. M. Tigelaar, R. A. Weiss and M. A. Meador, *ACS Nano*, 2012, **6**, 7644–7655.
14 Y. N. Meng, H. P. Wu, Y. J. Zhang and Z. X. Wei, *J. Mater. Chem. A*, 2014, **2**, 10842–10846.
15 T. Huang, R. G. Lu, C. Su, H. N. Wang, Z. Guo, P. Liu, Z. Y. Huang, H. M. Chen and T. S. Li, *ACS Appl. Mater. Interfaces*, 2012, **4**, 2699–2708.
16 J. Y. Wang, S. Y. Yang, Y. L. Huang, H. W. Tien, W. K. Chin and C. Ma, *J. Mater. Chem.*, 2011, **21**, 13569–13575.
17 C. Wei, L. M. Dai, A. Roy and T. B. Tolle, *J. Am. Chem. Soc.*, 2006, **128**, 1412–1413.
18 S. Z. Bisri, J. Gao, V. Derenskyi, W. Gomulya, I. Iezhokin, P. Gordiichuk, A. Herrmann and M. A. Loi, *Adv. Mater.*, 2012, **24**, 6147–6152.
19 V. Derenskyi, W. Gomulya, J. M. S. Rios, M. Fritsch, N. Fröhlich, S. Jung, S. Allard, S. Z. Bisri, P. Gordiichuk, A. Herrmann, U. Scherf and M. A. Loi, *Adv. Mater.*, 2014, **26**, 5969–5975.
20 Z. B. Yang, J. Deng, X. L. Chen, J. Ren and H. S. Peng, *Angew. Chem., Int. Ed.*, 2013, **52**, 13453–13457.
21 H. S. Fan, H. Wang, N. Zhao, X. L. Zhang and J. Xu, *J. Mater. Chem.*, 2012, **22**, 2774–2780.
22 H. Jiang, C. Z. Li, T. Sun and J. Ma, *Nanoscale*, 2012, **4**, 807–812.
23 C. G. Zhang, Z. W. Peng, J. Lin, Y. Zhu, G. D. Ruan, C. C. Hwang, W. Lu, R. H. Hauge and J. M. Tour, *ACS Nano*, 2013, **7**, 5151–5159.
24 J. F. Gao, D. X. Yan, H. D. Huang, X. B. Zeng, W. Q. Zhang and Z. M. Li, *J. Polym. Res.*, 2011, **18**, 2239–2243.
25 D. Li and R. B. Kaner, *Science*, 2008, **320**, 1170–1171.
26 L. Zhang, F. Zhang, X. Yang, G. K. Long, Y. P. Wu, T. F. Zhang, K. Leng, Y. Huang, Y. F. Ma, A. Yu and Y. S. Chen, *Sci. Rep.*, 2013, **3**, 1408.
27 Y. R. Li, K. X. Sheng, W. J. Yuan and G. Q. Shi, *Chem. Commun.*, 2013, **49**, 291–293.
28 X. C. Dong, G. C. Xing, M. B. Chan-Park, W. H. Shi, N. Xiao, J. Wang, Q. Y. Yan, T. C. Sum, W. Huang and P. Chen, *Carbon*, 2011, **49**, 5071–5078.
29 Z. J. Fan, J. Yan, L. J. Zhi, Q. Zhang, T. Wei, J. Feng, M. L. Zhang, W. Z. Qian and F. Wei, *Adv. Mater.*, 2010, **22**, 3723–3728.
30 S. Y. Yang, K. H. Chang, H. W. Tien, Y. F. Lee, S. M. Li, Y. S. Wang, J. Y. Wang, C. Ma and C. C. Hu, *J. Mater. Chem.*, 2011, **21**, 2374–2380.
31 F. Du, D. S. Yu, L. M. Dai, S. Ganguli, V. Varshney and A. K. Roy, *Chem. Mater.*, 2011, **23**, 4810–4816.
32 M. K. Liu, C. Zhang, W. W. Tjiu, Z. Yang, W. Z. Wang and T. X. Liu, *Polymer*, 2013, **54**, 3124–3130.

33 L. Yu, J. S. Park, Y. S. Lim, C. S. Lee, K. Shin, H. J. Moon, C. M. Yang, Y. S. Lee and J. H. Han, *Nanotechnology*, 2013, **24**, 155604.
34 C. Y. Tang, G. C. Long, X. Hu, K. W. Wong, W. M. Lau, M. K. Fan, J. Mei, T. Xu, B. Wang and D. Hui, *Nanoscale*, 2014, **6**, 7877–7888.
35 J. Kim, T. Kim, J. W. Suk, H. Chou, J. Jang, J. H. Lee, I. N. Kholmanov, D. Akinwande and R. S. Ruoff, *Small*, 2014, **10**, 3405–3411.
36 C. Zhang, S. Huang, W. W. Tjiu, W. Fan and T. X. Liu, *J. Mater. Chem.*, 2012, **22**, 2427–2434.
37 Z. B. Yang, M. K. Liu, C. Zhang, W. W. Tjiu, T. X. Liu and H. S. Peng, *Angew. Chem., Int. Ed.*, 2013, **52**, 3996–3999.
38 M. K. Liu, Y. E. Miao, C. Zhang, W. W. Tjiu, Z. B. Yang, H. S. Peng and T. X. Liu, *Nanoscale*, 2013, **5**, 7312–7320.
39 X. Yang, F. Zhang, L. Zhang, T. F. Zhang, Y. Huang and Y. S. Chen, *Adv. Funct. Mater.*, 2013, **23**, 3353–3360.
40 X. Yang, L. Zhang, F. Zhang, T. F. Zhang, Y. Huang and Y. S. Chen, *Carbon*, 2014, **72**, 381–386.
41 N. Wu, X. L. She, D. J. Yang, X. F. Wu, F. B. Su and Y. F. Chen, *J. Mater. Chem.*, 2012, **22**, 17254–17261.
42 N. D. Luong, U. Hippi, J. T. Korhonen, A. J. Soininen, J. Ruokolainen, L. Johansson, J. Nam, L. H. Sinh and J. Seppälä, *Polymer*, 2011, **52**, 5237–5242.
43 J. D. Rancourt and L. T. Taylor, *Macromolecules*, 1987, **20**, 790–795.
44 X. R. Wang, Y. Si, X. F. Wang, J. M. Yang, B. Ding, L. Chen, Z. M. Hu and J. Y. Yu, *Nanoscale*, 2013, **5**, 886–889.
45 Y. Si, X. M. Tang, J. L. Ge, S. Yang, M. El-Newehy, S. S. Al-Deyab, J. Y. Yu and B. Ding, *Nanoscale*, 2014, **6**, 2102–2105.
46 X. F. Wang, B. Ding, G. Sun, M. R. Wang and J. Y. Yu, *Prog. Mater. Sci.*, 2013, **58**, 1173–1243.
47 Y. Wang, Z. X. Shi and J. Yin, *J. Phys. Chem. C*, 2010, **114**, 19621–19628.
48 D. V. Kosynkin, A. L. Higginbotham, A. Sinitskii, J. R. Lomeda, A. Dimiev, B. K. Price and J. M. Tour, *Nature*, 2009, **458**, 872–875.
49 N. D. Luong, U. Hippi, J. T. Korhonen, A. J. Soininen, J. Ruokolainen, L. S. Johansson, J. D. Nam, L. H. Sinh and J. Seppala, *Polymer*, 2011, **52**, 5237–5242.
50 J. Dong, C. Q. Yin, X. Zhao, Y. Z. Li and Q. H. Zhang, *Polymer*, 2013, **54**, 6415–6424.
51 Y. Xu, S. H. Wang, Z. T. Li, Q. Xu and Q. H. Zhang, *J. Mater. Sci.*, 2013, **48**, 7863–7868.
52 W. Yuan, J. Feng, Z. Judeh, J. Dai and M. B. Chan-Park, *Chem. Mater.*, 2010, **22**, 6542–6554.
53 S. Ramakrishnan, M. Dhakshnamoorthy, E. J. Jelmy, R. Vasanthakumari and N. K. Kothurkar, *RSC Adv.*, 2014, **4**, 9743–9749.